JOURNAL OF VIROLOGY, Sept. 2007, p. 9525–9535 Vol. 81, No. 17
0022-538X/07/$08.00+0 doi:10.1128/JVI.02503-05


# X-Ray Crystal Structures of Human Immunodeficiency Virus Type 1 Protease Mutants Complexed with Atazanavir▽†

Herbert E. Klei,[1]* Kevin Kish,[1] Pin-Fang M. Lin,[5] Qi Guo,[5,6] Jacques Friborg,[5] Ronald E. Rose,[5] Yaqun Zhang,[2,3] Valentina Goldfarb,[2] David R. Langley,[4] Michael Wittekind,[2,3]‡ and Steven Sheriff[1]

*Macromolecular Crystallography,[1] Macromolecular NMR,[2] and Gene Expression & Protein Biochemistry,[3] Bristol-Myers Squibb Pharmaceutical Research Institute, Princeton, New Jersey 08543-4000; Computer Assisted Drug Design[4] and Virology,[5] Bristol-Myers Squibb Pharmaceutical Research Institute, Wallingford, Connecticut 06492-7660; and Applied Genomics, Bristol-Myers Squibb Pharmaceutical Research Institute, Hopewell, New Jersey 08534-2130[6]*

Received 30 November 2005/Accepted 22 May 2007

**Atazanavir, which is marketed as REYATAZ, is the first human immunodeficiency virus type 1 (HIV-1) protease inhibitor approved for once-daily administration. As previously reported, atazanavir offers improved inhibitory profiles against several common variants of HIV-1 protease over those of the other peptidomimetic inhibitors currently on the market. This work describes the X-ray crystal structures of complexes of atazanavir with two HIV-1 protease variants, namely, (i) an enzyme optimized for resistance to autolysis and oxidation, referred to as the cleavage-resistant mutant (CRM); and (ii) the M46I/V82F/I84V/L90M mutant of the CRM enzyme, which is resistant to all approved HIV-1 protease inhibitors, referred to as the inhibitor-resistant mutant. In these two complexes, atazanavir adopts distinct bound conformations in response to the V82F substitution, which may explain why this substitution, at least in isolation, has yet to be selected in vitro or in the clinic. Because of its nearly symmetrical chemical structure, atazanavir is able to make several analogous contacts with each monomer of the biological dimer.**

The human immunodeficiency virus type 1 (HIV-1) protease (PRT) enzyme is essential for viral replication. As such, it is an attractive target for antiviral therapy. Indeed, a sustained, international effort of structure-based drug design has led to the development of potent HIV-1 PRT inhibitors (PIs) that bind to the active site of mature PRT. Several of these drugs are currently in use for the treatment of AIDS (18, 31, 36). The seven FDA-approved PIs currently on the market (in order of approval [http://www.fda.gov/oashi/aids/virals.html])—saquinavir, ritonavir, indinavir, nelfinavir, amprenavir, lopinavir, and atazanavir—are competitive peptidomimetics (10, 15). Unfortunately, the use of these PIs can lead to rapid selection for drug-resistant PRT variants (1, 42, 50). Mutations of the conserved PRT residues V82, I84, and L90 are among those most commonly observed in patients receiving PI-containing regimens. In addition, the collective data from clinical failures of antiviral therapy show considerable cross-resistance among the PIs (19). Both factors threaten the long-term effectiveness of these drugs. Therefore, it is important to understand the mechanisms that govern drug resistance in order to develop more effective inhibitors and to rationally formulate drug regimens.

Atazanavir, a highly potent azapeptide, is the most recently approved HIV-1 PI. A favorable pharmacokinetic profile allows once-daily dosing (37, 43, 47). More importantly, atazanavir has a distinct resistance profile relative to those of the other approved PIs. Earlier in vitro studies demonstrated that the substitutions M46I, A71V, N88S, I84V, and I50L, which were identified in laboratory strains of PRT variants selected against atazanavir, may play important roles in the resistance phenotype and that multiple mutational pathways can lead to resistance (17). In clinical studies of treatment-experienced patients who received atazanavir-containing regimens, a reduction in atazanavir susceptibility required combinations of several amino acid substitutions (7). High levels of atazanavir resistance were observed only with HIV isolates cross-resistant to all approved PIs, and these viruses were characterized by the accumulation of several mutations (M46I, I84V, N88S/D, and L90M). These studies also identified the signature I50L mutation in treatment-naïve patients who failed atazanavir therapy. Although data are limited due to the overall low frequency (<2%) of atazanavir-resistant isolates, the I50L mutation was identified in 100% of subjects classified as having virological failure. However, unlike other resistance mutations, the presence of the I50L mutation in clinical isolates obtained from these treatment-naïve patients was associated with increased susceptibility and no cross-resistance to the other six approved PIs (8). Phenotypic studies of engineered HIV strains containing the I50L mutation and cell-based PRT assays (8, 62) also demonstrated this increased susceptibility to other PIs. Recent calorimetric studies have also indicated increased binding affinities of the I50L mutation-containing PRT for all approved PIs except atazanavir, correlating well with the hypersusceptibility phenotype (67). While the clinical significance of these observations is still under investigation, the emergence of the I50L mutation during atazanavir therapy may potentially preserve future PI-based treatment options.

* Corresponding author. Mailing address: Bristol-Myers Squibb, P.O. Box 4000, Princeton, NJ 08543-4000. Phone: (609) 252-4359. Fax: (609) 252-6030. E-mail: herbert.klei@bms.com.

† Supplemental material for this article may be found at http://jvi.asm.org/.

‡ Present address: Amgen, 1201 Amgen Court West, Seattle, WA 98119-3105.

▽ Published ahead of print on 30 May 2007.

Detailed information from the crystallographic analysis of HIV-1 PRT-inhibitor complexes has played a major role in the structure-based development of potent inhibitors (57, 63, 64). To better define the mechanism of action and the drug resistance phenotypes associated with atazanavir, we determined the X-ray crystal structures of two PRT variants complexed with atazanavir, namely, (i) an enzyme optimized for resistance to autolysis and oxidation, referred to as the cleavage-resistant mutant (CRM); and (ii) the PI-resistant M46I/V82F/I84V/L90M quadruple mutant of the CRM enzyme, referred to as the inhibitor-resistant mutant (IRM). The loss of PRT susceptibility of viral isolates with the IRM mutations to the approved PIs, atazanavir included, varied between 7- and 71-fold (17). The M46I and L90M substitutions were associated with atazanavir resistance in clinical studies (7). Furthermore, the V82F and I84V subset, especially when present in tandem, has been shown to adversely affect PRT susceptibility (17, 23, 55). This work reports the structural characterization of an alternative binding mode of atazanavir to HIV-1 PRT in response to the V82F substitution, which is not associated with atazanavir resistance unless it is present in combination with several other mutations.

## MATERIALS AND METHODS

**Cloning.** A pET3b-PRT construct that was codon optimized for *Escherichia coli* was obtained from Tang et al. (21). This original PRT construct, referred to as TANG, was subjected to several rounds of mutagenesis. Using the procedure reported by Kunkel (24), four amino acid substitutions, namely, L10I, I13V, S37N, and R41K, were introduced to duplicate the published PRT RF gene (54). Two additional steps were taken to make the protein more amenable to structural biology. First, since uninhibited wild-type PRT is susceptible to autolysis, three more amino acid substitutions, Q7K, L33I, and L63I, were introduced to confer autolysis resistance as reported by Mildner et al. (30) and Rosé et al. (44). This construct is referred to as RF-AUTO. Second, to overcome the tendency of wild-type PRT to form disulfide-linked multimers, two more amino acid substitutions, C67A and C95A, were introduced to generate the RF-AUTO-C construct (33, 60, 61, 65, 66). The PRT product of the RF-AUTO-C gene is referred to as the CRM. A final round of mutagenesis incorporated four additional amino acid substitutions away from the wild-type PRT sequence, namely, M46I, V82F, I84V, and L90M, and yielded the RF-AUTO-C-I construct. The PRT product of the RF-AUTO-C-I gene is referred to as the IRM because, when present together, these four substitutions alter the cleavage activity of the protein and render the PRT resistant to all currently approved PIs (17, 26, 34, 56). The CRM and IRM proteins were used in the structural studies. The final proteins had favorable biophysical properties (were cysteine-free, autocatalysis resistant, and well folded) and were shown to be active on standard substrates by in vitro assay. All mutagenesis procedures were performed with standard molecular biology methods (for details, see Appendix SA in the supplemental material). The sequences of the constructs were verified by DNA sequence analysis. The protein and DNA sequences of the above series of mutants are summarized in Appendix SB in the supplemental material.

**Expression and purification.** The pET24d-RF-AUTO-C (CRM) and pET24d-RF-AUTO-C-I (IRM) plasmids were inserted into *E. coli* BL21(DE3) host cells. Procedures similar to those described by Ohtaka et al. (34) and Yanchunas et al. (67) were used to express and purify these proteins. For the CRM protein, the yield was approximately 20 mg/liter of culture, with a refolding efficiency of 80%. The activity assay and $^{1}H$-$^{15}N$ HSQC nuclear magnetic resonance (NMR) spectrum indicated that the protein was active and folded when routinely concentrated to 22 mg/ml and, on occasion, as high as 40 mg/ml. For the IRM protein, a poorer yield of 1 mg/liter of culture was obtained. In addition, for storage, IRM fractions were pooled and concentrated to approximately 1 mg/ml after sodium dodecyl sulfate-polyacrylamide gel electrophoresis analysis. Detailed procedures are given in Appendix SC in the supplemental material.

**Crystallization.** All complexes were generated by cocrystallization by the hanging-drop vapor diffusion method at room temperature. The CRM and IRM protein solutions consisted of 9.0 mg/ml protein buffered by 20 mM sodium acetate, pH 5.5, incubated with 4.7 mM inhibitor (approximately 10× molar excess). An evenly spaced six-by-eight grid of reservoir solutions, i.e., 20 to 45% saturated ammonium sulfate in 5% increments (4.1 M taken as 100% saturated) by pH 4.6 to 7.4 in increments of 0.4, was used to screen for crystallization conditions. Based on experience gained from earlier crystallization trials, the grid was designed to center successful conditions between the extremes. Similar, more focused grids over smaller ranges were frequently used to further refine the growth conditions. The optimal CRM reservoir conditions were 27.25 parts (vol/vol) 0.1 M sodium citrate and 72.75 parts (vol/vol) 0.2 M disodium monohydrogen phosphate (resulted in pH 6.6) with 30% saturated ammonium sulfate (9, 29). The same conditions worked well for the IRM reservoir; however, many other conditions based on the same ingredients also grew crystals. A reservoir volume of 1 ml and a drop volume of 2 μl (1:1 ratio of protein and reservoir solutions) were used. Once the 1 μl of reservoir solution for each drop was withdrawn, 40 μl of 0.1 M β-mercaptoethanol, 40 μl of isopropanol, and 100 μl of dimethyl sulfoxide were added to each reservoir (S. Foundling, personal communication). Although de novo crystals were readily grown, seeding—both micro and macro—was used to improve the likelihood of crystallization and to increase the crystal size. Large crystals of up to 1 mm in length, suitable for diffraction measurements, typically grew within 3 days. A 20% (vol/vol) glycerol solution prepared with the reservoir solution was used as the cryoprotectant. Additional details are given in Appendix SD in the supplemental material.

**Data collection. (i) CRM.** Diffraction images were recorded on an R-Axis II image plate detector mounted on a Rigaku RU-200 X-ray generator run at 50 kV and 100 mA (5 kW), with Yale/MSC mirrors focused at 200 mm. A collimator with 0.5- by 1.0-mm pinholes was used to render the CuKα beam sufficiently colinear. An Oxford Cryosystems model 600 liquid nitrogen cooler maintained the mounted crystal at 100 K. The images were processed with the HKL suite (35). The crystals exhibited symmetry consistent with space group $P2_12_12_1$, with unit cell dimensions as follows: $a$ = 51.2 Å, $b$ = 58.2 Å, and $c$ = 61.3 Å. Diffraction data were recorded over the resolution range of 40.0 to 1.8 Å.

**(ii) IRM.** Diffraction images were collected at the IMCA-CAT 17-ID beamline at the Advanced Photon Source, Argonne National Laboratory, Chicago, IL, tuned to 1.0-Å radiation. A Bruker two-by-two-mosaic charge-coupled device detector set to the 1-K binned mode was used to record the images, while the cold stream from an Oxford Cryosystems model 600 liquid nitrogen cooler maintained the mounted crystal at 100 K. The images were processed with HKL2000 (35). The crystals exhibited symmetry consistent with space group $P2_12_12_1$, with unit cell dimensions as follows: $a$ = 53.4 Å, $b$ = 58.2 Å, and $c$ = 61.3 Å. Although diffraction data were observed to beyond a 1.5-Å resolution, in the interest of throughput, collection was limited to one sweep, with 2θ only slightly offset. Complete data were recorded only over the resolution range of 20.0 to 1.6 Å. The statistics for the processed diffraction data for both structures are given in Table 1.

**Refinement. (i) CRM.** Prior to refinement, the structure factors were placed on an approximate absolute scale by the method of Sheriff and Hendrickson per their equation 3 (53). The structure was determined by molecular replacement with the program AMoRe (32), with 1HVI used as the search model.

**(ii) IRM.** Prior to refinement, the structure factors were placed on an approximate absolute scale with TRUNCATE (16) in conjunction with several other auxiliary CCP4 (6) routines. The structure was determined by molecular replacement with the program AMoRe (32), with the CRM structure used as the search model.

**(iii) General.** The structures were initially refined by several cycles of model building with CHAIN (45) and refinement with X-PLOR (3). In preparation for publication, both structures were further refined with CNX (release 2002; Accelrys, Inc., San Diego, CA) to make the structures consistent, except as dictated by electron density. The program QUANTA (QUANTA Modeling Environment, release 2000; Accelrys, Inc., San Diego, CA) was used for model building. The programs PROCHECK (25) and MolProbity (27) were used to flag suspect features, with deference given to MolProbity. Overall refinement statistics from CNX are presented in Table 2.

**Structural analysis. (i) Selection of structures.** X-ray crystal structures of the FDA-approved peptidomimetic PIs complexed with PRT available as of 2 September 2004 were downloaded from the Protein Data Bank (PDB) (2). The HIV Structural Database maintained by the National Institute of Standards and Technology (http://xpdb.nist.gov/hivsdb/hivsdb.html) and its precursor, the HIV Protease Database posted by the National Cancer Institute (http://mcl1.ncifcrf.gov/hivdb/index.html), were also utilized in the search (58). Structures of PI analogues and fragments, such as 1K6P, 1K6T, and 1K6V for indinavir, were not included. The presence of the inhibitor was verified by inspection. A total of 21 structures, including 18 PI complexes (indinavir, 1HSG, 2BPX, 1C6Y, 1K6C, 1SDT, 1SDU, and 1SDV; ritonavir, 1HXW and 1N49; nelfinavir, 1OHR; saquinavir, 1HXB, 1FB7, 1C6Z, and 1MTB; amprenavir, 1HPV; and lopinavir,

TABLE 1. Measures of diffraction quality[a]

| Parameter | Value for CRM | | | Value for IRM | | |
|---|---|---|---|---|---|---|
| | Overall | First shell | Last shell | Overall | First shell | Last shell |
| Resolution range (Å) | 40.0–1.80 | 40.0–3.88 | 1.86–1.80 | 20.0–1.60 | 20.0–3.44 | 1.66–1.60 |
| Total no. of observations | 72,994 | ≥8,883 | ≥3,703 | 87,023 | ≥7,938 | ≥4,531 |
| Unique no. of observations | 17,386 | 1,880 | 1,519 | 25,238 | 2,567 | 2,234 |
| Redundancy | 4.2 | ≥4.7 | ≥2.4 | 3.4 | ≥3.1 | ≥2.0 |
| $R_{merge}$ (%) | 4.7 | 2.8 | 14.1 | 6.9 | 6.2 | 29.8 |
| $I/\sigma(I)$ | 30.7 | 48.6 | 6.7 | 17.5 | 19.9 | 2.7 |
| Completeness (%) | 98.2 | 98.5 | 87.3 | 97.5 | 92.9 | 87.5 |
| Mosaicity (°) | 0.48–0.76 | | | 0.39–0.42 | | |
| No. (%) of rejections | 0 (0.0) | | | 450 (0.5) | | |

[a] A Perl script, read_scalepack.pl, written by Steven Sheriff was used to extract these statistics from SCALEPACK (35) output.

1MUI), 1 CA-p2 complex (1F7A), and 2 apo structures (2HVP and 3HVP) were identified.

**(ii) Alignment of sequences.** The full-length PRT sequences were easily aligned by inspection because of the high degree of sequence identity between the PRT variants. A list of residues in which at least one of the selected structures differed from the consensus wild-type sequence taken from 1HVI was compiled (Table 3). To aid in the structural analysis, this list of residues was populated with wild-type residues as needed, and the pseudo sequences were arranged by mutation pattern with the GCG PileUp (11; Wisconsin GCG package, version 10.3; Accelrys, Inc. San Diego, CA) and Vector NTI AlignX/ClustalW (suite 8; InforMax/Invitrogen, Carlsbad, CA) programs.

**(iii) Alignment of structures.** Three-dimensional structures were superimposed with the program ALIGN (48), complemented by numerous internal programs and CCP4 (6) routines. The inhibitor structures were overlaid on 1F7A (structure of PRT complexed with the 10-mer fragment KARVLAEAMS of the CA-p2 natural substrate). 1F7A was selected as the reference structure because the P4-to-P4′ features of CA-p2 have been described in detail (39) and the directionality of the CA-p2 peptide is clear. Dimer asymmetry was used to guide superposition. The orientation with the lowest Cα root mean square deviation (RMSD) was used to define the P3-to-P3′ directionality for each inhibitor, with one exception. For 1MTB, the orientation that best aligned saquinavir with nelfinavir from 1OHR was used. For cases in which the two monomers of the PRT dimer are related by noncrystallographic symmetry and two inhibitor conformations are given (1HXB and 1C6Z for saquinavir and 1MUI for lopinavir), the low RMSD alignment was used since the directionality of the ligand with respect to the dimer asymmetry is purportedly bidirectional. In the case of 1FB7 for saquinavir, the symmetry between the two monomers in the biological dimer is crystallographic, so the two orientations are indistinguishable.

When multiple related structures of protein-ligand complexes are compared, they are typically superimposed based on Cα or main-chain protein atoms. Outliers are then often ignored to better align conserved cores. In the case of monomeric, or even heteromeric, assemblies, this superposition is straightforward—the protein coordinates are superimposed and the ligands are positioned by the same transformation. However, in the case of HIV-1 PRT, due to the homodimeric nature of the protein and the quasi-symmetric nature of the PIs, it is not as obvious how to align structures for comparison. For many of the

TABLE 2. Refinement results[a]

| Statistic | Value for CRM | | Value for IRM | |
|---|---|---|---|---|
| Model contents and quality of fit | Overall | Last shell | Overall | Last shell |
| Resolution range (Å) | 39.3–1.8 | 1.88–1.80 | 19.7–1.6 | 1.67–1.60 |
| No. of reflections | 17,318 | 1,906 | 25,196 | 2,691 |
| $R$ (%) | 16.9 | 17.8 | 23.5 | 36.7 |
| $R_{free}$ (%) | 20.2 | 23.7 | 24.6 | 36.5 |
| No. of protein atoms | 1,514 | | 1,529 | |
| No. of heterogen atoms | 102 (atazanavir) | | 51 (atazanavir) | |
| No. of solvent atoms | 256 (225 HOH, 3 SUL, 2 GOL, 1 ACT)[b] | | 202 (193 HOH, 1 SUL, 1 ACT) | |
| RMSD bond length (Å) | 0.012 | | 0.009 | |
| RMSD bond angle (°) | 1.7 | | 1.2 | |
| RMSD improper angle (°) | 0.7 | | 0.8 | |
| Mean B factor (Å$^2$) | 15.9 | | 21.1 | |
| Estimates of coordinate error | | | | |
| Estimated coordinate error | ESD[c] | Cross-validated ESD | ESD | Cross-validated ESD |
| Luzzati method | 0.16 | 0.21 | 0.22 | 0.24 |
| Sigmaa method | 0.07 | 0.15 | 0.19 | 0.20 |
| Avg atom-to-atom changes in B factor | | | | |
| Isotropic B-factor restraint | RMS | Sigma | RMS | Sigma |
| No. of main-chain bonds | 1.1 | 1.5 | 1.3 | 1.5 |
| No. of main-chain angles | 1.6 | 2.0 | 2.0 | 2.0 |
| No. of side-chain bonds | 2.0 | 2.0 | 1.8 | 2.0 |
| No. of side-chain angles | 2.8 | 2.5 | 2.6 | 2.5 |

[a] Values were gathered from the PDB file output by the CNX (Accelrys, Inc.) (3) script xtal_pdbsubmission.inp.
[b] HOH, water; SUL, sulfate anion; GOL, glycerol; ACT, acetate anion.
[c] ESD, estimated standard deviation.

TABLE 3. Amino acid substitutions in PRT structures sorted by sequence homology[a]

| PI[b] | PDB accession no. | Amino acid substitution at position[c] | | | | | | | | | | | | | | | | | | | | |
|---|---|---|---|---|---|---|---|---|---|---|---|---|---|---|---|---|---|---|---|---|---|---|
| | | I3 | Q7 | L10 | I13 | K14 | K20 | L24 | D25 | L33 | S37 | R41 | **M46** | G48 | I54 | L63 | I64 | C67 | A71 | **V82** | **I84** | **L90** | C95 |
| RTV | 1HXW | | | | | | | | | | M | | | | | | | | | | | | |
| SQV | 1HXB | V | | | | | | | | | | | | | | | | | | | | | |
| SQV | 1FB7 | V | | | | | | | | | | | | V | | | | | | | | M | |
| IDV | 1SDT | | K | | | | | | | I | | | | | | I | | A | | | | | A |
| IDV | 1SDU | | K | | | | | | | I | | | | | | I | | A | | | | M | A |
| IDV | 1SDV | | K | | | | | | | I | | | | | | I | | A | | A | | | A |
| ATV | 2FXE (CRM) | | K | I | V | | | | | I | N | K | | | | I | | A | | | | | A |
| ATV | 2FXD (IRM) | | K | I | V | | | | | I | N | K | I | | | I | | A | | F | V | M | A |
| SQV | 1C6Z | | | V | | | M | I | | | D | | I | | V | P | | | V | T | | | |
| IDV | 1C6Y | | | V | | | M | I | | | D | | I | | V | P | | | V | T | | | |
| SQV | 1MTB | | | | | R | | | N | | N | K | | | | P | V | | | | | | |
| CA-p2 | 1F7A | | K | | | R | | | N | | N | K | | | | P | V | | | | | | |
| RTV | 1N49 | | K | | | R | | | N | | N | K | | | | P | V | | | A | | | |
| IDV | 1K6C | | K | | | R | | | | | N | | | | | P | | | | T | V | | |
| Apo | 2HVP | | | | | | | | | | N | | | | | | | | | | | | |
| Apo | 3HVP | | | | | R | | | | | N | K | | | | P | V | B | | | | | B |

[a] The data were arranged to cluster mutation patterns with more "wild-type" sequences toward the top, except for the apo entries, which were placed at the bottom. The following amino acid sequences agree with the consensus wild-type sequence (1HVI) and are therefore not shown: 1HSG and 2BPX for indinavir, 1OHR for nelfinavir, 1HPV for amprenavir, and 1MUI for lopinavir. Residues 67 and 95 of the apo PDB entry 3HVP, marked as B, are α-amino-*N*-butyric acid.

[b] RTV, ritonavir; SQV, saquinavir; IDV, indinavir; ATV, atazanavir.

[c] Positions shown in bold are those which differentiate IRM from CRM.

commercially available PIs, the effective N-to-C-terminal directionality of each individual peptidomimetic is ambiguous because plausible N–Cα–CO atoms, or pseudo atoms, can be assigned in either direction. Such is especially true for atazanavir because of its high degree of quasi-symmetry. Furthermore, no crystallographic requirement exists to consistently assign chain identifications to the two molecules in the biological dimer from one structure to the next or even within structures with multiple dimers in the asymmetric unit (e.g., 1N49 for ritonavir). Typically, software used to align structures pairs atoms in the order of input. Atoms are not treated as constellations to be superimposed irrespective of order. In the PRT literature, PI orientations are largely, but not completely, consistent (40, 67). To resolve this ambiguity, the asymmetry of the protein dimer was found to be a reliable discriminator between alternative superpositions of PRT complexes, with one exception, 1MTB, which happens to be the only structure with saquinavir modeled in just one conformation. Conformational changes in response to mutations do not explain this outlier because the sequences of 1F7A and 1MTB are identical except for a K7Q substitution. A more detailed analysis of the 1MTB refinement and size, shape, and charge complementarities may be able to explain this discrepancy.

**(iv) Clinical relevance.** In addition to specific articles referenced in the text, the HIV Drug Resistance Database maintained by Stanford University (http://hivdb.stanford.edu) was used to correlate mutations with clinical susceptibility (41).

**Protein database accession numbers.** The coordinates for the CRM and IRM structures were deposited in the PDB under entries 2FXE and 2FXD, respectively.

## RESULTS

**Viability of protein used for structural studies.** As previously described (67), the catalytic activities of the HIV-1 CRM and IRM PRTs were analyzed by chromogenic peptide cleavage in the presence of five of the currently FDA-approved PIs (all but amprenavir and lopinavir). All of the 50% inhibitory concentrations ($IC_{50}$s) against the CRM PRT were determined to be in the range of 0.68 to 0.91 nM, whereas with the IRM PRT the $IC_{50}$s were 12 nM for atazanavir, 34 nM for saquinavir, 59 nM for ritonavir, 96 nM for nelfinavir, and 115 nM for indinavir. Therefore, the CRM and IRM PRTs were considered to be active and appropriately susceptible to PIs to be used for structural studies.

**Structure of HIV PRT in complex with atazanavir.** The structure of at least one PRT complex is available from the PDB (2) for each of the PIs on the market. In this study, the X-ray crystal structures of the HIV-1 CRM and IRM PRTs complexed with atazanavir (Fig. 1) were determined. The two atazanavir complexes reported here crystallized in one of the more common PRT crystal forms, i.e., space group $P2_12_12_1$, with unit cell dimensions as follows: $a \approx 52$ Å, $b \approx 58$ Å, and $c \approx 61$ Å. Six structures for four of the seven FDA-approved PIs also crystallized in this form (for atazanavir, 2FXE and 2FXD; for saquinavir, 1MTB; for indinavir, 1K6C and 1SDU; and for nelfinavir, 1OHR). Except for the most recent indinavir structures (1SDT, 1SDU, and 1SDV), the resolutions of the structures reported here—CRM at 1.8 Å and IRM at 1.6 Å—are toward the higher end for deposited structures. The correlation between improved resolution and the more recent structures is probably attributable to the increased use of cryotechniques and synchrotron sources. In terms of global folding, all PRT structures are fundamentally the same. Even with sequence and inhibitor variation, with all 198 residues taken into account, the Cα RMSDs from structure 1F7A for the dimers ranged only from 0.3 to 0.8 Å. All of the CRM and IRM mutations from the consensus wild-type sequence of 1HVI are also present in at least one of the reference structures, with the exception of I13V (Table 3). Five of the reference structures (1HSG and 2BPX for indinavir, 1OHR for nelfinavir, 1HPV for amprenavir, and 1MUI for lopinavir) have the wild-type sequence. The Cα deviations of the CRM monomers from the wild-type structures are no more than the deviation within this set. Therefore, despite the nine amino acid substitutions (Q7K, L10I, I13V, L33I, S37N, R41K, L63I, C67A, and C95A) compared to the wild-type sequence, the CRM structure can be considered a wild-type structure. The surface Lys and Glu residues for which the entire side chain could not be modeled were consistent with those from structures of other PI com-

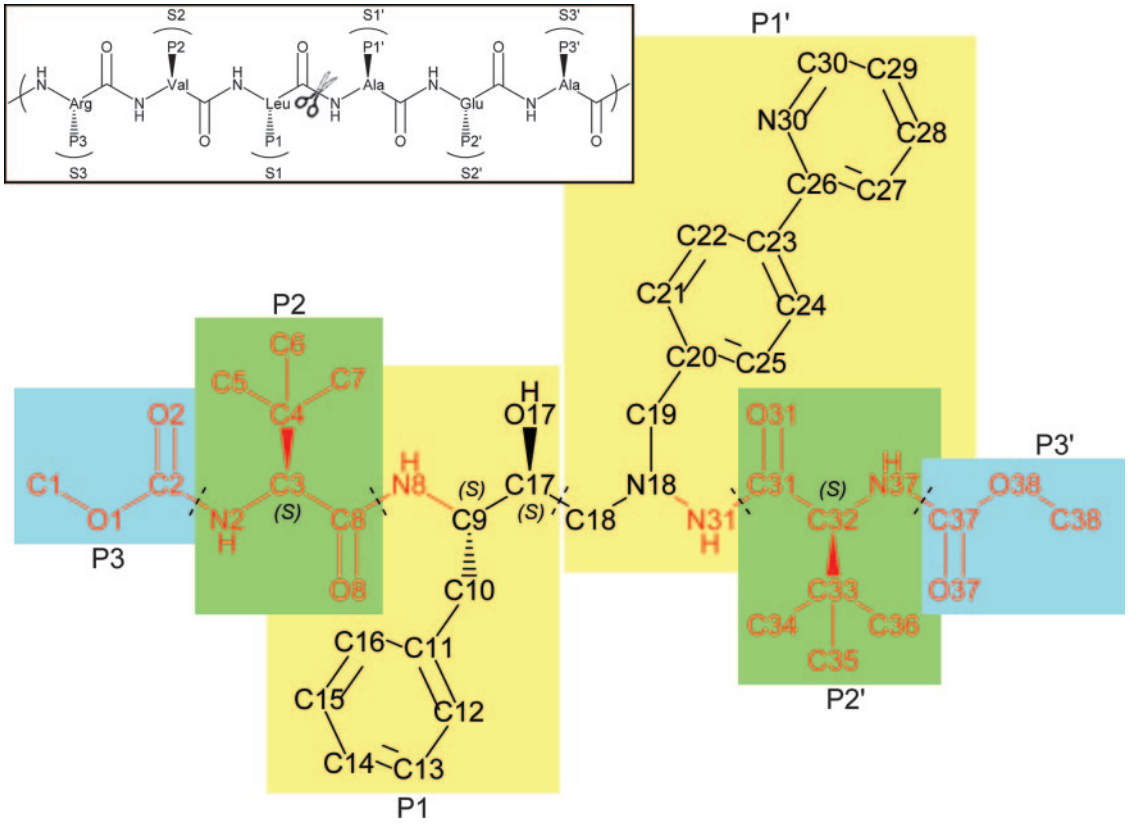


FIG. 1. Chemical structure of atazanavir, which is marketed as the sulfuric acid salt under the trade name REYATAZ, with the section attributed to each PRT subsite highlighted and labeled in accordance with standard nomenclature (49). Atom labels are as found in the CRM and IRM structures. The common group found at each end is colored red. All four chiral centers, as indicated by wedge bonds, are in the *S* configuration. The IUPAC name for atazanavir is (3*S*,8*S*,9*S*,12*S*)-3,12-bis(1,1-dimethylethyl)-8-hydroxy-4,11-dioxo-9-(phenylmethyl)-6-[[4-(2-pyridinyl)phenyl]methyl]-2,5,6,10,13-pentaazatetradecanedioic acid dimethyl ester, although it can also be described as 1-[4-(pyridin-2-yl)phenyl]-5(*S*)-2,5-bis{[*N*-(methoxy-carbonyl)-L-*tert*-leucinyl]amino}-4(*S*)-hydroxy-6-phenyl-2-azahexane because of its peptidic nature. The molecular mass of the free base, $C_{38}H_{52}N_6O_7$, is 704.9 Da (802.9 Da for the sulfuric acid salt). A schematic of the CA-p2 peptide fragment from 1F7A is included for reference. During the deposition process, the atom names for atazanavir 1FXE and 1FXD were changed to match those used in 2AQU (5). A conversion table is given in Appendix SG of the supplemental material.

plexes (see Appendix SE in the supplemental material). Yet, in terms of discrete disorder, relatively few residues with alternate conformations were noted compared to other structures of similar or higher resolution (see Appendix SF in the supplemental material). Two such residues, Ile66 and Ile72, both from monomer A, were unique to the IRM structure. In the IRM structure, atazanavir was bound in only one orientation with the pyridyl moiety on the prime side (monomer A), but in the CRM structure, atazanavir was bound in two orientations, as also seen by Clemente et al. (5) and analogous to 1HXB and 1C6Z for saquinavir and 1MUI for lopinavir.

**Atazanavir binds in two orientations in the CRM structure.** The electron density for the refined CRM structure is indicative of an alternate atazanavir orientation (Fig. 2), much like that in 1HXB and 1C6Z for saquinavir, 1MUI for lopinavir, and 2AQU for atazanavir (5). Even though both the CRM and IRM proteins crystallized in the same space group with similar unit cell dimensions, their crystal packing is very different in terms of some key intermolecular contacts. With the IRM structure in this lattice, the Phe82/pyridine-driven distortion limits atazanavir to only one orientation in the IRM structure. When residue 82 is Val, as in the CRM structure, this distortion cascade does not occur. Consequently, in the CRM dimer, atazanavir can be accommodated in either orientation. These differences demonstrate the interplay between inhibitor geometry, protein sequence, quaternary structure, and crystal packing.

**Distinction between global and local effects.** The differences in the two monomers in response to the pyridyl asymmetry of atazanavir are illustrative of the distinction between local and global effects. As already shown by the pronounced distortion of residues 79 to 82 of monomer A compared to residues 79 to 82 of monomer B, the displacements in the IRM structure to accommodate both Phe82 and the pyridyl ring connected at C23, but not C14, are localized. In the IRM structure, the Cα RMSD between all 99 residues of the two monomers, at 0.9 Å, is the largest of those for any of the compared structures (0.7 Å for 1C6Y is the second largest). Yet if the residues whose deviations are >1.8 Å (residues 17, 67 to 69, and 80 to 82) are treated as outliers, the IRM intradimer RMSD drops to 0.6 Å, which is consistent with 0.5 Å for the same subset of CRM residues.

In contrast, the relative displacement of monomers A and B used to assign ligand directionality is a global effect. Compared to the 3HVP apo biological dimer, the monomers in the PI

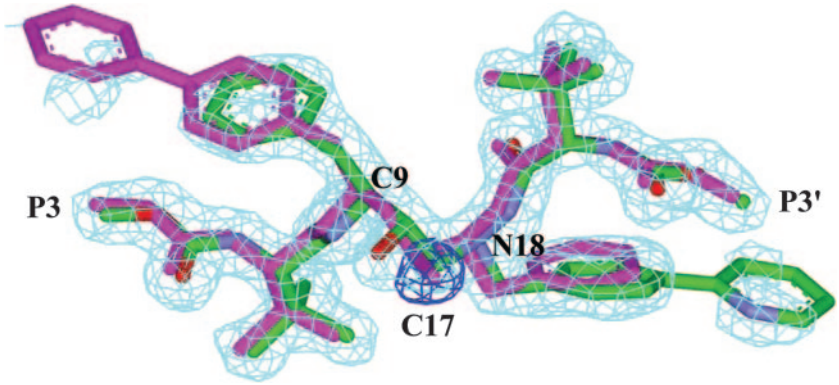


FIG. 2. Electron density interpreted as an alternate conformation for atazanavir in the CRM structure. The alternate conformation was generated by the superposition of CRM on itself, with monomers A and B swapped (Cα RMSD of 0.6 Å). Atazanavir superimposes on itself remarkably well when reversed due in part to the ability of the $sp^3$ N18 to approximate the chiral carbon C9. The $F_0$-$F_c$ difference electron density contoured at +3σ (blue) for the hydroxyl oxygen off the central chiral center at C17 is modeled very nicely by the alternate conformation. Also, unlike the bulk of atazanavir, the $2F_0$-$F_c$ electron density contoured at +1σ (cyan) for the pyridyl ring is incomplete in both locations, suggestive of partial occupancies associated with the alternate conformation. Atoms are labeled as in Fig. 1. The image was generated with the program Discovery Studio Modeling (release 1.1; Accelrys, Inc., San Diego, CA).

complexes are rotated approximately 10° with respect to each other. A detectable directionality is associated with this rotation. Relative to all 198 residues of the CRM dimer, the IRM dimer Cα RMSD of 0.8 Å is the largest for the examined structures. Yet despite this apparent dissimilarity, the CRM and IRM structures exhibit similar global asymmetry. The superposition of the CRM coordinates on those of 1F7A, both as deposited and with the order of the monomers reversed in the PDB file, gives values of 0.46 and 0.60 Å, respectively (Δ = 0.14 Å). The same numbers for the IRM coordinates are 0.63 and 0.76 Å, respectively (Δ = 0.13 Å). This directionality is attributable to the consistent rotation of one monomer relative to the other between structures.

**Alternative atazanavir binding mode in response to V82F substitution.** Several reports have previously analyzed and/or predicted the effects of various point mutations on the catalytic activity, inhibition, and structural stability of PRT (10, 14, 22, 52). This analysis will focus on the V82F mutation, for which the CRM and IRM structures provide clear insight. For atazanavir, unlike other PIs, the V82F mutation has yet to be selected in vitro (17) or observed in the clinic (7, 41) unless it is present in combination with three or more other mutations. The V82F mutation appears to be better tolerated by atazanavir, which could be due to its ability to bind in different conformations depending on which amino acid is present at residue 82 (Fig. 3). In the CRM structure, Val82 forms a hydrophobic pocket (P1/P1′) along with Leu23 and Ile84. The phenylpyridyl moiety points between $Arg8_A$ (subscript "A" refers to monomer A) and $Pro81_A$ toward the solvent. In the IRM structure, $Phe82_A$ π-stacks with the pyridyl ring of atazanavir (ring interplanar distance, 3.8 Å), which causes residues $79_A$ to $83_A$ to move away from the binding site. The phenylpyridyl moiety rotates 67° around the N18–C19 bond (and also 20° around the C19–C20 bond) in order to move into the hydrophobic pocket created by $Leu23_A$ and $Ile84_A$ as it aligns with the side chain of $Phe82_A$. The pyridyl moiety is partially

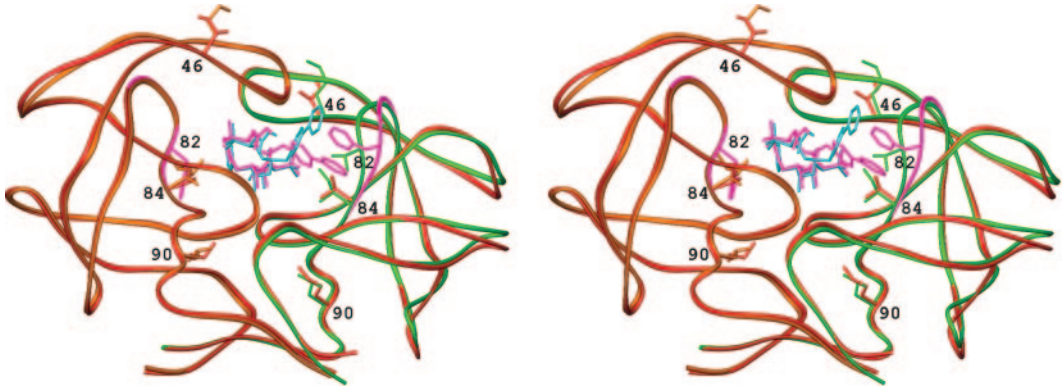


FIG. 3. Stereo overlay of the CRM (monomer A, green; monomer B, orange) and IRM (residues 78 to 82, magenta; other residues, red) complexes with atazanavir. Side chains for the four CRM-to-IRM amino acid substitutions (M46I, V82F, I84V, and L90M) are similarly colored. Atazanavir (CRM, cyan; IRM, magenta) is positioned below the flaps which fold across the top. In the CRM structure, the phenylpyridyl moiety of atazanavir points between $Arg8_A$ and $Phe81_A$ (not shown) toward the solvent. In contrast, in the IRM structure, the pyridyl group π-stacks with $Phe82_A$. Similar distortion of monomer B is not observed because no pyridyl group is present at C14, unlike C23 (see Fig. 1). The image was prepared with the program RIBBONS (4).

TABLE 4. Cα deviations between the superimposed CRM and IRM structures[a]

| Residue or substitution | Cα deviation (Å) | | |
|---|---|---|---|
| | Monomer A | Monomer B | \|A − B\| |
| K14 | 0.9 | 0.4 | 0.5 |
| I15 | 0.9 | 0.5 | 0.4 |
| G16 | 1.6 | 0.7 | 0.9 |
| G17 | 2.3 | 1.2 | 1.1 |
| Q18 | 1.9 | 0.7 | 1.2 |
| L19 | 1.5 | 0.5 | 1.0 |
| K20 | 0.9 | 0.2 | 0.7 |
| M36 | 0.7 | 0.9 | 0.2 |
| N37 | 1.5 | 1.4 | 0.1 |
| L38 | 1.4 | 1.6 | 0.2 |
| P39 | 2.3 | 1.9 | 0.4 |
| G40 | 1.7 | 2.3 | 0.5 |
| K41 | 0.8 | 1.4 | 0.6 |
| W42 | 0.4 | 1.0 | 0.6 |
| K43 | 0.3 | 1.4 | 1.1 |
| P44 | 0.6 | 1.1 | 0.5 |
| **M46I** | 0.7 | 0.6 | 0.1 |
| I66 | 1.5 | 0.1 | 1.4 |
| A67 | 2.8 | 0.3 | 2.5 |
| G68 | 2.5 | 0.4 | 2.1 |
| H69 | 1.8 | 0.1 | 1.7 |
| K70 | 1.1 | 0.2 | 0.9 |
| P79 | 0.9 | 0.5 | 0.4 |
| T80 | 1.5 | 0.4 | 1.1 |
| P81 | 3.1 | 0.7 | 2.4 |
| **V82F** | 2.2 | 0.8 | 1.4 |
| **I84V** | 0.3 | 0.2 | 0.1 |
| **L90M** | 0.4 | 0.3 | 0.1 |

[a] Except for the four mutations between the CRM and IRM sequences (in bold), only residues for which at least one of the deviations exceeded 0.8 Å are shown. The rightmost column of double differences highlights residues for which the quality of the superposition differs between the A and B monomers. In addition to the large differences at residues 79 to 82, the differences at residues 66 to 69 appear to be caused by the formation of a hydrogen bond between His69 ND1 and a symmetry-related Gly51 O which draws this loop in monomer A of the IRM structure closer to its neighbor than is the case for monomer A of the CRM structure or monomer B of either structure.

buried by the surface created by Phe82$_A$. These rearrangements represent more than minor steric shifts. They represent two distinct binding modes in response to an amino acid substitution. When Ala is present at residue 82 instead of Phe, this compensatory rearrangement of the phenylpyridine is not advantageous. Minor adjustment of the atazanavir pseudo-backbone torsion angles between P2 and P2′ allows the distal ends of atazanavir in the CRM and IRM structures to be placed in much the same orientation (Fig. 3), despite the conformational differences at P1′. This alternative binding mode is consistent with the ±V82F mutant activity reported by Clemente et al. (5).

**Importance of V82F substitution.** The V82F substitution is of particular importance in the IRM structure. Of the four CRM-to-IRM mutations (M46I, V82F, I84V, and L90M), the V82F mutation is the only one associated with significant Cα displacement between the superimposed CRM and IRM structures (Table 4). In the presence of atazanavir, the main-chain displacement of Phe82$_A$ displaces Pro81$_A$, which, at 3.1 Å, represents the largest Cα displacement. Pro81$_A$, in turn, displaces the position of the symmetry-related Trp6$_B$ and other nearby residues. Only the PRT monomer near the pyridyl moiety, monomer A, is subject to this local distortion. The configurations of monomer B are much the same in the CRM and IRM structures. The Cα displacements for residues 79 to 82 of monomer B are of the same magnitude as those for the bulk of the protein, which illustrates the localized nature of the distortion cascade driven by the Phe82$_A$-pyridine interaction.

**Packing around residues 46, 84, and 90.** In addition to the V82F mutation described above, the CRM and IRM proteins differ at three other positions, including the I84V mutation, which has been associated with both in vivo and in vitro resistance (7, 8, 51), and the M46I and L90M mutations. In the CRM and IRM complexes with atazanavir, the environment around residue 84 in monomer A differs principally due to (i) the Phe82/pyridine-related rearrangement in the IRM complex and (ii) atazanavir being bound in two opposite orientations in

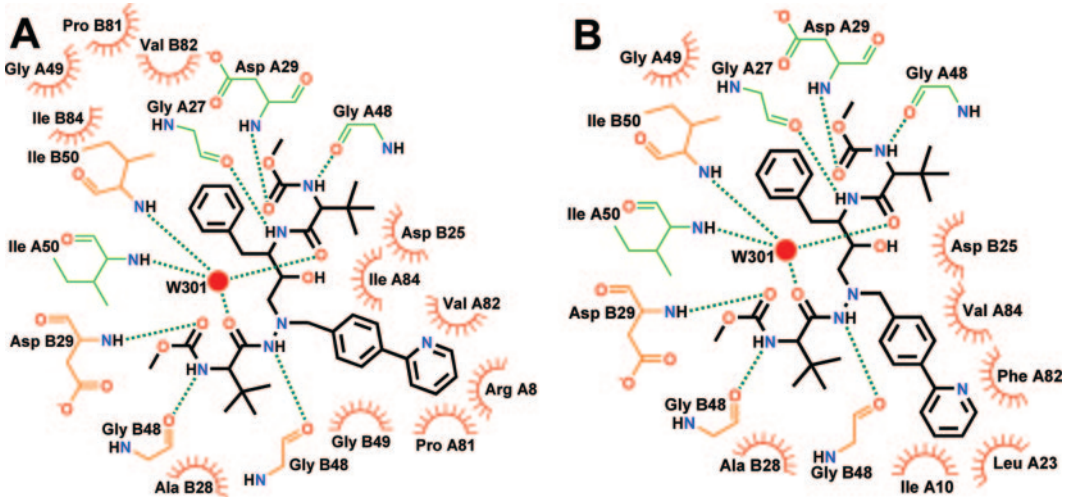


FIG. 4. Two-dimensional schematics of the interactions between atazanavir and PRT in the CRM (A) and IRM (B) structures. The quasi-symmetry of atazanavir (black) is reflected in its contacts. Residues from monomers A and B are colored green and orange, respectively. Hydrogen bonds are shown as dashed dark green lines (refer to Tables 5 and 6 for interatomic distances). Hydrogen bonds between the central hydroxyl of atazanavir and Asp25, the catalytic aspartic acid, of each monomer were omitted for clarity. A key conserved water molecule, W301 (red sphere), sits between the Ile50 residues of the A and B monomers. The figure was created with the program LIGPLOT (59) and rearranged with ChemDraw.

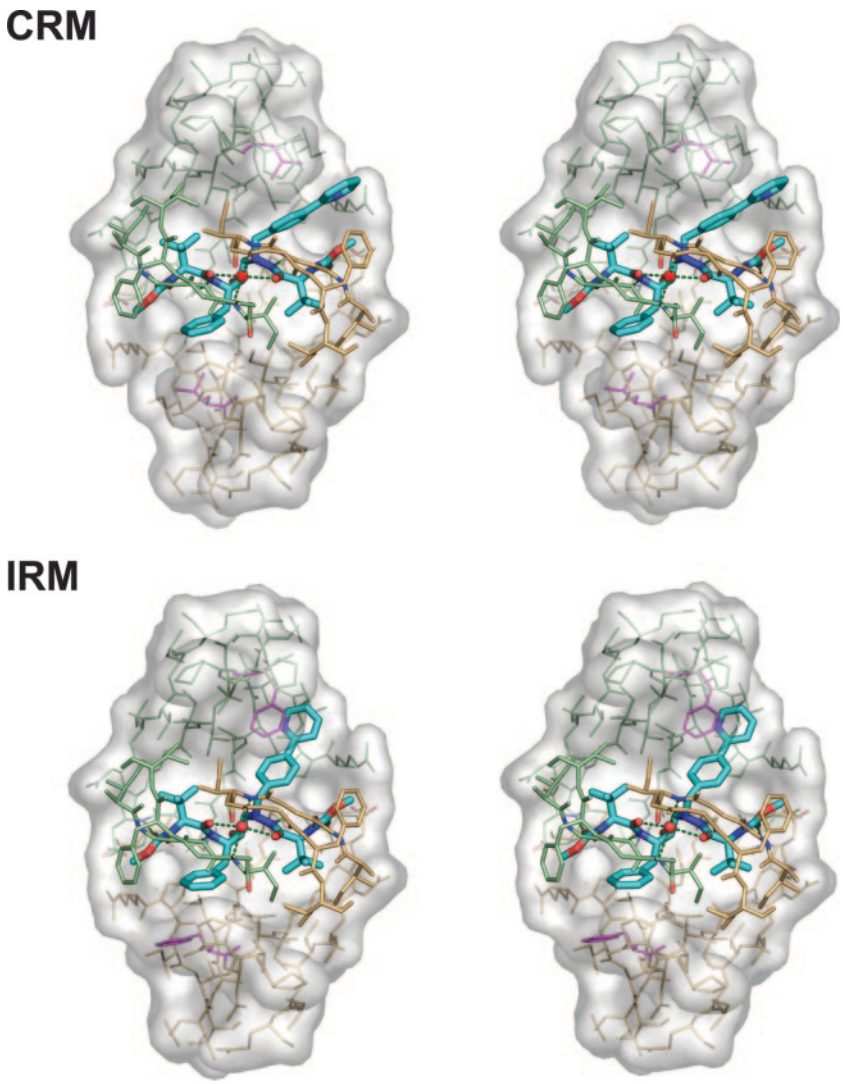


FIG. 5. Stereo illustration of the interactions between atazanavir and PRT in the CRM (top) and IRM (bottom) structures. The quasi-symmetry of atazanavir (cyan) is reflected in its contacts. Monomers A and B are colored green and orange, respectively. Hydrogen bonds are shown as dashed dark green lines (refer to Tables 5 and 6 for interatomic distances). The view is down the noncrystallographic twofold axis of the dimer shown from the flap side. A key conserved water molecule, W301 (red sphere), sits between the Ile50 residues of the A and B monomers and is positioned on the noncrystallographic twofold axis located at the center. Residue 82 from each monomer is highlighted in magenta. Flap residues 47 to 54, which lie above the inhibitor and were omitted from the protein surface calculation, were drawn with thicker bonds than the underlying protein. The image was prepared with the program PyMOL (DeLano Scientific, San Carlos, CA).

the CRM complex. In monomer A of both the CRM and IRM structures, the side chains of Asp25, Ala28, and Val(Phe)82 are within 4 Å of the side chain of Ile(Val)84. Moreover, pseudo-symmetrically related atoms C10 (C19) of the linker to the phenyl rings and C7 (C35) of the *t*-butyls from the two different atazanavir orientations are within 4 Å of Ile84, as is C12 of conformer B in the CRM structure. In the IRM structure, atoms from the phenyl portion of the phenylpyridyl moiety, i.e., C21, which pseudo-symmetrically corresponds to C12, and C22, interact with Val84. However, the similarities in the CRM and IRM structures outweigh any differences. In monomer B of CRM, the interactions of Ile84 resemble those of monomer A due to the different orientations of atazanavir, but in monomer B of IRM, with just one atazanavir orientation, Val84 interacts only with Asp25.

Residue 46 is part of the flap, and its side chain is on the surface. In both the CRM and IRM structures, residue 46 of monomer A points towards the aliphatic portion of a symmetry-related Lys70 from monomer B, whereas residue 46 of monomer B points towards Ile72 from a symmetry-related monomer A.

Finally, in three of the four monomers, the side chain of residue 90 (Leu in CRM and Met in IRM) is within 4 Å of the same sets of residues, including (i) Leu5 from the other monomer of the homodimer and (ii) Leu24 and Ile85 from the same monomer. Only in monomer B of the IRM structure are the interactions different, where the Met90 side chain is within 4 Å of the side chain of only Ala95. However, even here, this apparent difference is more a function of the arbitrary nature of the distance cutoff, as CRM Leu90 and IRM Met90 occupy much the same space when the structures are superimposed.

TABLE 5. Direct atazanavir-PRT hydrogen bonds, with interatomic distances, observed in the CRM and IRM complexes

| Protein monomer | Atazanavir atom-PRT atom | Interatomic distance (Å) | |
|---|---|---|---|
| | | CRM | IRM |
| A | O17–Asp25 OD1 | 3.0 | 2.9 |
| | O17–Asp25 OD2 | 3.0 | 2.6 |
| | O2–Asp29 N | 3.0 | 3.0 |
| | N2–Gly48 O | 2.9 | 2.9 |
| | N8–Gly27 O | 3.3 | 3.1 |
| B | O17–Asp25 OD1 | 2.6 | 2.6 |
| | O17–Asp25 OD2 | 2.9 | 3.2 |
| | O37–Asp29 N | 2.9 | 3.0 |
| | N37–Gly48 O | 3.0 | 2.9 |
| | N31–Gly27 O | 3.1 | 3.0 |

[a] For simplicity, only the primary monomer (alternate conformer A) of atazanavir in the CRM structure is reported. However, the same trend is observed for alternate conformer B. But for the catalytic aspartic acid, Asp25, of each monomer, only main-chain protein atoms form direct hydrogen bonds with atazanavir.

## DISCUSSION

**Comparison of the relative binding affinities of various PIs to the CRM and IRM PRTs.** All PIs, atazanavir included, were less potent against the IRM PRT than against the CRM PRT. However, the potency loss was at least threefold less with atazanavir than with the other PIs. Moreover, the $IC_{50}$ values are consistent with those published in a study by Clemente et al. (5) in which three pairs of ±V82F PRTs were assayed for activity by chromogenic cleavage against all seven FDA-approved PIs. None of the ±V82F PRTs contained any of the other three IRM substitutions. With the notable exception of atazanavir, all of the PIs exhibited either weak or diminished inhibition against one or more of the F82 PRTs. Thus, at least for these cases, PRT susceptibility to atazanavir was retained in the presence of an isolated V82F substitution.

**Exploitation of quasi-symmetry.** The quasi-palindromic chemistry of atazanavir is more pronounced than that of any of the other six approved HIV-1 PIs. Both the P2-P3 and P2′-P3′ ends of atazanavir contain *N*-(methoxycarbonyl)-L-*tert*-leucine [-NH-CO-$C(CH_3)_3$-NH-CO-O-$CH_3$]. This quasi-symmetry is reflected in its molecular contacts with the PRT dimer (Fig. 4 and Fig. 5). Hydrogen bonds between atazanavir and PRT are the same for both monomers A and B (Table 5). Except for the central hydroxyl (O17), all inhibitor-protein hydrogen bonds in both the CRM and IRM structures involve the duplicated portion of atazanavir. Furthermore, but for OD1 and OD2 of Asp25, only backbone amide nitrogen atoms and carbonyl oxygen atoms of residues 27, 29, and 48 make direct hydrogen bonds with atazanavir; therefore, one might expect mutations at these residues to have less of an impact on atazanavir inhibition of HIV-1 PRT than would be the case if their side chains made specific interactions with the ligand. Of the seven marketed PIs, atazanavir is the only one to make such extensive direct hydrogen-bonding interactions with main-chain atoms. In this regard, it most closely resembles the peptide bound in the 1F7A structure, which forms 10 hydrogen bonds to main-chain atoms (38). In fact, the only main-chain hydrogen bonds formed with the peptide but not atazanavir are with Gly48 N. Atazanavir, saquinavir, and ritonavir form hydrogen bonds with $Gly48_A$ O. However, because of its higher degree of quasi-symmetry, atazanavir is the only marketed PI that also forms a hydrogen bond with $Gly48_B$ O. These hydrogen bonds are important for substrate recognition. For example, a protein with the G48V mutation retained 50 to 80% of wild-type activity with cleavage-site peptides (28). In contrast, a protein with the V82S mutation, whose side chain makes hydrophobic interactions with inhibitors and therefore, presumably, substrates, retained only 2 to 20% of wild-type activity. In vivo saquinavir resistance has been linked to two mutations, namely, G48V and L90M, as well as the G48V/L90M double mutant (20). The increase in $K_i$ compared to that of the wild-type enzyme (14) was attributed to the Val48 side chain displacing the inhibitor farther from the PRT, resulting in a larger gap between the inhibitor P3 moiety and the S3 subsite contained in the flap region of the enzyme (20).

Water-mediated hydrogen bonds are also largely conserved (Table 6). This similarity extends to hydrophobic interactions between the protein and the repeated *t*-butyl and methyl ester groups. In contrast, the hydrophobic interactions between the protein and the core inhibitor phenyl and 2-phenylpyridyl substituents show some uniqueness with their respective mono-

TABLE 6. Water-mediated hydrogen bonds, with interatomic distances, observed in the CRM and IRM complexes[a]

| Protein monomer | Atazanavir atom-HOH molecule-PRT atom | Interatomic distance (Å) | | | |
|---|---|---|---|---|---|
| | | CRM | | IRM | |
| | | Atazanavir to $H_2O$ | $H_2O$ to protein atom | Atazanavir to $H_2O$ | $H_2O$ to protein atom |
| A | O1–W212–Gly48 O | | | 3.0 | 3.0 |
| | O1–W24–Gly48 N | 3.4 | 2.8 | 3.2 | 2.7 |
| | O2–W7–Asp29 OD1 | 3.2 | 2.7 | 3.3 | 2.8 |
| | O2–W7–Gly27 O | 3.2 | 2.9 | 3.3 | 2.8 |
| | O8–W301–Ile50 N | 2.7 | 2.8 | 2.8 | 2.9 |
| | O31–W301–Ile50 N | 2.7 | 2.8 | 2.8 | 2.9 |
| B | O38–W162–Gly48 O | 3.3 | 2.8 | | |
| | O37–W6–Asp29 OD1 | 3.3 | 2.8 | 3.1 | 2.8 |
| | O37–W6–Gly27 O | 3.3 | 3.0 | 3.1 | 3.0 |
| | O31–W301–Ile50 N | 2.7 | 3.0 | 2.8 | 3.0 |
| | O8–W301–Ile50 N | 2.7 | 3.0 | 2.8 | 3.0 |
| Atazanavir-atazanavir | O-8–W301–O31 | 2.7 | 2.8 | 2.8 | 2.8 |

[a] The high degree of quasi-symmetry of the ligand and of the PRT dimer is reflected in the interatomic interactions in terms of both the atoms and distances involved. Similarly situated waters in both structures (e.g., W301) were assigned the same residue number to aid in such comparisons. A 3.3-Å cutoff was used, although entries above this value were included to complete rows.

mers. The ability of PRT to accommodate additional ligand symmetry when available raises the question of whether this feature could be exploited further to obtain more potent and/or more resistant inhibitors. For instance, perhaps the chirality at the scissile bond could be relaxed. While the use of symmetry in the design of PIs is not new (12, 13), the implication of this quasi-symmetry is still not fully understood.

**I50L mutation and atazanavir resistance.** The clinical link between the I50L mutation and atazanavir resistance was discovered after these structural studies were completed. In the absence of structures of Leu50-PRT–PI complexes, modeling studies (67) were done based on the CRM and IRM structures, both of which contain Ile50. $Ile50_A$ and $Ile50_B$ are located between the S1-S2′ and S2-S1′ binding sites and interact with the P1-P2′ and P2-P1′ groups of the PIs, respectively. These Ile residues also coordinate the conserved water found in the structures of most, if not all, PRT-PI complexes, even those determined in solution by NMR (60, 61). Analogous to these other structures, the conserved water (labeled W301) mediates hydrogen bonds between the amide groups of $Ile50_A$/$Ile50_B$ and the O8/O31 carbonyl oxygen atoms of atazanavir (Table 6 and Fig. 4). Therefore, since this conserved water interacts similarly with all PIs and its protein contact is limited to the backbone amide nitrogen of residue 50, its role appears to be conserved across PIs. Thus, subtle changes to the environment of the conserved water were not considered to be the principal reason behind the atazanavir-specific resistance linked to the I50L mutation. Rather, in the case of atazanavir, the large *t*-butyl groups at P2 and P2′ form close van der Waals contacts with $Ile50_B$ and $Ile50_A$, respectively. An I50L substitution would introduce steric clash to these otherwise favorable interactions. To relieve the clash, the flaps must undergo conformational changes to accommodate atazanavir. These changes, which were predicted to be more pronounced for P2′ than for P2, would slightly open the active site and result in reduced binding affinity (67). The I50L resistance substitution is more readily accommodated by the PIs with smaller substituents at P2 and/or P2′. Fortunately, unlike other resistance substitutions, the I50L mutation is associated with increased susceptibility and no cross-resistance to other approved PIs (8). Thus, even if I50L mutation-based atazanavir resistance is encountered, it can potentially be addressed with other readily available PIs.

**Conclusions.** This work presents the X-ray crystal structures of two mutant forms of HIV-1 PRT complexed with atazanavir. Atazanavir was shown to take advantage of its quasi-symmetric chemistry and the homodimeric nature of the target in terms of binding interactions. This work also highlights the ability of atazanavir to adopt a different but effective binding mode in direct response to the clinically relevant V82F mutation. This ability of atazanavir to adopt a different conformation in the presence of the V82F mutation bodes well for the clinical use of atazanavir as a component of highly active antiretroviral therapy against the AE strain of HIV, where this particular mutation is routinely found and against which Clemente et al. (5) have shown that atazanavir, in comparison to all other PIs, remains potent in vitro.

## ACKNOWLEDGMENTS

We thank Jordan Tang, head of the Protein Studies Research Program at the Oklahoma Medical Research Foundation, for the initial HIV-1 PRT vector. Critical reviews of the manuscript by several colleagues at Bristol-Myers Squibb, namely, Patricia McDonnell, John Sack, Paul Morin, Chong-Hwan Chang, and Eric Baldwin, and also by the anonymous referees are very much appreciated. We thank Matthew Cahn and Malcolm Davis for several useful Python and Perl scripts to assemble information from the large collection of PRT-related PDB entries.

The diffraction experiments were done through the Industrial Macromolecular Crystallography Association-Collaborative Access Team (IMCA-CAT). IMCA is an association of pharmaceutical companies committed to the use of macromolecular crystallography in drug discovery and product development to which Bristol-Myers Squibb belongs. The Center for Synchrotron Radiation Research and Instrumentation at the Illinois Institute of Technology was contracted to construct and operate the beamlines, biochemistry laboratory, offices, and other resources within the facility.

Use of the Advanced Photon Source was supported by the U.S. Department of Energy, Office of Science, Office of Basic Energy Sciences, under contract W-31-109-Eng-38.

## REFERENCES

1. **Ala, P. J., E. E. Huston, R. M. Klabe, D. D. McCabe, J. L. Duke, C. J. Rizzo, B. D. Korant, R. J. DeLoskey, P. Y. S. Lam, C. N. Hodge, and C.-H. Chang.** 1997. Molecular basis of HIV-1 protease drug resistance: structural analysis of mutant proteases complexed with cyclic urea inhibitors. Biochemistry **36:**1573–1580.
2. **Berman, H. M., J. Westbrook, Z. Feng, G. Gilliland, T. N. Bhat, H. Weissig, I. N. Shindyalov, and P. E. Bourne.** 2000. Protein data bank. Nucleic Acids Res. **28:**235–242.
3. **Brünger, A. T., P. D. Adams, G. M. Clore, W. L. DeLano, P. Gros, R. W. Grosse-Kunstleve, J.-S. Jiang, J. Kuszewski, M. Nilges, N. S. Pannu, R. J. Read, L. M. Rice, T. Simonson, and G. L. Warren.** 1998. Crystallography & NMR system: a new software suite for macromolecular structure determination. Acta Crystallogr. D **54:**905–921.
4. **Carson, M.** 1997. RIBBONS. Methods Enzymol. **277:**493–505.
5. **Clemente, J. C., R. M. Coman, M. M. Thiaville, L. K. Janka, J. A. Jeung, S. Nukoolkarn, L. Govindasamy, M. Agbandje-McKenna, R. McKenna, W. Leelamanit, M. M. Goodenow, and B. M. Dunn.** 2006. Analysis of HIV-1 CRF_01 A/E protease inhibitor resistance: structural determinants for maintaining sensitivity and developing resistance to atazanavir. Biochemistry **45:**5468–5477.
6. **Collaborative Computational Project Number 4.** 1994. The CCP4 suite: programs for protein crystallography. Acta Crystallogr. D **50:**760–763.
7. **Colonno, R. J., A. Thiry, K. Limoli, and N. Parkin.** 2003. Activities of atazanavir (BMS-232632) against a large panel of human immunodeficiency virus type 1 clinical isolates resistant to one or more approved protease inhibitors. Antimicrob. Agents Chemother. **47:**1324–1333.
8. **Colonno, R., R. Rose, C. McLaren, A. Thiry, N. Parkin, and J. Friborg.** 2004. Identification of I50L as the signature atazanavir (ATV)-resistance mutation in treatment-naïve HIV-1-infected patients receiving ATV-containing regimens. J. Infect. Dis. **189:**1802–1810.
9. **Dawson, R. M. C., D. C. Elliott, W. H. Elliot, and K. M. Jones.** 1986. Data for biochemical research, 3rd ed. Clarendon Press, Oxford, United Kingdom.
10. **De Clercq, E.** 2002. New developments in anti-HIV chemotherapy. Biochim. Biophys. Acta **1587:**258–275.
11. **Devereux, J., P. Haeberli, and O. Smithies.** 1984. A comprehensive set of sequence analysis programs for the VAX. Nucleic Acids Res. **12:**387–395.
12. **Erickson, J., D. J. Neidhart, J. VanDrie, D. J. Kempf, X. C. Wang, D. W. Norbeck, J. J. Plattner, J. W. Rittenhouse, M. Turon, N. Wideburg, W. E. Kohlbrenner, R. Simmer, R. Helfrich, D. A. Paul, and M. Knigge.** 1990. Design, activity, and 2.8 Å crystal structure of a $C_2$ symmetric inhibitor complexed to HIV-1 protease. Science **249:**527–533.
13. **Erickson, J. W.** 1993. Design and structure of symmetry-based inhibitors of HIV-1 protease, p. 109–128. *In* P. S. Anderson, G. L. Kenyon, and G. R. Marshall (ed.), Perspectives in drug discovery and design. ESCOM Science, Leiden, The Netherlands.
14. **Ermolieff, J., X. Lin, and J. Tang.** 1997. Kinetic properties of saquinavir-resistant mutants of human immunodeficiency virus type 1 protease and their implications in drug resistance *in vivo*. Biochemistry **36:**12364–12370.
15. **Flexner, C.** 1998. HIV-protease inhibitors. N. Engl. J. Med. **338:**1281–1292.
16. **French, S., and K. Wilson.** 1978. On the treatment of negative intensity observations. Acta. Crystallogr. A **34:**517–525.
17. **Gong, Y.-F., B. S. Robinson, R. E. Rose, C. Deminie, T. P. Spicer, D. Stock, R. J. Colonno, and P.-F. Lin.** 2000. In vitro resistance profile of the human immnunodeficiency virus type 1 protease inhibitor BMS-232632. Antimicrob. Agents Chemother. **44:**2319–2326.
18. **Gulick, R. M.** 1997. Current antiretroviral therapy: an overview. Quality Life Res. **6:**471–474.
19. **Hertogs, K., S. Bloor, S. D. Kemp, C. V. den Eynde, T. M. Alcorn, R. Pauwels, M. V. Houtte, S. Staszewski, V. Miller, and B. A. Larder.** 2000.

Phenotypic and genotypic analysis of clinical HIV-1 isolates reveals extensive protease inhibitor cross-resistance: a survey of over 6000 samples. AIDS **14:**1203–1210.
20. **Hong, L., X. C. Zhang, J. A. Hartsuck, and J. Tang.** 2000. Crystal structure of an in vivo HIV-1 protease mutant in complex with saquinavir: insights into the mechanisms of drug resistance. Protein Sci. **9:**1898–1904.
21. **Ido, E., H.-P. Han, F. J. Kezdy, and J. Tang.** 1991. Kinetic studies of human immunodeficiency virus type 1 protease and its active-site hydrogen bond mutant A28S. J. Biol. Chem. **266:**24359–24366.
22. **Kagan, R. M., M. D. Shenderovich, P. N. R. Heseltine, and K. Ramnarayan.** 2005. Structural analysis of an HIV-1 protease I47A mutant resistant to the protease inhibitor lopinavir. Protein Sci. **14:**1870–1878.
23. **Klabe, R. M., L. T. Bacheler, P. J. Ala, S. Erickson-Viitanen, and J. L. Meek.** 1998. Resistance to HIV protease inhibitors: a comparison of enzyme inhibition and antiviral potency. Biochemistry **37:**8735–8742.
24. **Kunkel, T. A.** 1985. Rapid and efficient site-specific mutagenesis without phenotype selection. Proc. Natl. Acad. Sci. USA **82:**488–492.
25. **Laskowski, R. A., M. W. MacArthur, D. S. Moss, and J. M. Thornton.** 1993. PROCHECK: a program to check the stereochemical quality of protein structures. J. Appl. Crystallogr. **26:**283–291.
26. **Lin, Y., X. Lin, L. Hong, S. Foundling, R. L. Heinrikson, S. Thaisrivongs, W. Leelamanit, D. Raterman, M. Shah, B. M. Dunn, and J. Tang.** 1995. Effect of point mutations on the kinetics and the inhibition of human immunodeficiency virus type 1 protease: relationship to drug resistance. Biochemistry **34:**1143–1152.
27. **Lovell, S. C., I. W. Davis, W. B. Arendall III, P. I. W. de Bakker, J. M. Word, M. G. Prisant, J. S. Richardson, and D. C. Richardson.** 2003. Structure validation by Cα geometry: ϕ, ψ and Cβ deviation. Proteins **50:**437–450.
28. **Mahalingam, B., Y.-F. Wang, P. I. Boross, J. Tozser, J. M. Louis, R. W. Harrison, and I. T. Weber.** 2004. Crystal structures of HIV protease V82A and L90M mutants reveal changes in the indinavir-binding site. Eur. J. Biochem. **271:**1516–1524.
29. **McIlvaine, T. C.** 1921. A buffer solution for colorimetric comparison. J. Biol. Chem. **49:**183–186.
30. **Mildner, A. M., D. J. Rothrock, J. W. Leone, C. A. Bannow, J. M. Lull, I. M. Reardon, J. L. Sarcich, W. J. Howe, C. C. Tomich, C. W. Smith, R. L. Heinrikson, and A. G. Tomasselli.** 1994. The HIV-1 protease as enzyme and substrate: mutagenesis of autolysis sites and generation of a stable mutant with retained kinetic properties. Biochemistry **33:**9405–9413.
31. **Molla, A., G. R. Granneman, E. Sun, and D. J. Kempf.** 1998. Recent developments in HIV protease inhibitor therapy. Antivir. Res. **39:**1–23.
32. **Navaza, J.** 1994. AMoRe: an automated package for molecular replacement. Acta Crystallogr. A **50:**157–163.
33. **Nicholson, L. K., T. Yamazaki, D. A. Torchia, S. Grzesiek, A. Bax, S. J. Stahl, J. D. Kaufman, P. T. Wingfield, P. Y. S. Lam, P. K. Jadhav, C. N. Hodge, P. J. Domaille, and C.-H. Chang.** 1995. Flexibility and function in HIV-1 protease. Struct. Biol. **2:**274–280.
34. **Ohtaka, H., A. Schön, and E. Freire.** 2003. Multidrug resistance to HIV-1 protease inhibition requires cooperative coupling between distal mutations. Biochemistry **42:**13659–13666.
35. **Otwinowski, Z., and W. Minor.** 1997. Processing of X-ray diffraction data collected in oscillation mode. Methods Enzymol. **276:**307–326.
36. **Palella, F. J., K. M. Delaney, A. C. Moorman, M. O. Loveless, J. Fuhrer, G. A. Satten, D. J. Aschman, and S. D. Holmberg.** 1998. Declining morbidity and mortality among patients with advanced human immunodeficiency virus infection. N. Engl. J. Med. **338:**853–860.
37. **Piliero, P., P. Cahn, G. Pantaleo, J. M. Gatell, K. Squires, L. Percival, I. Sanne, R. Wood, P. Phanuphak, S. Shelton, A. Lazzarin, A. Thiry, T. Kelleher, M. Giordano, and S. M. Schnittman.** 2002. Atazanavir: a once-daily protease inhibitor with a superior lipid profile: results of clinical trials beyond week 48, abstr. 706-T. Abstr. 9th Conf. Retrovir. Opportun. Infect.
38. **Pivazyan, A. D., D. S. Matteson, L. Fabry-Asztalos, R. P. Singh, P.-F. Lin, W. Blair, K. Guo, B. Robinson, and W. H. Prusoff.** 2000. Inhibition of HIV-1 protease by a boron-modified polypeptide. Biochem. Pharmacol. **60:**927–936.
39. **Prabu-Jeyabalan, M., E. Nalivaika, and C. A. Schiffer.** 2000. How does a symmetric dimer recognize an asymmetric substrate? A substrate complex of HIV-1 protease. J. Mol. Biol. **301:**1207–1220.
40. **Prabu-Jeyabalan, M., E. A. Nalivaika, N. M. King, and C. A. Schiffer.** 2003. Viability of a drug-resistant human immunodeficiency virus type 1 protease variant: structural insights for better antiviral therapy. J. Virol. **77:**1306–1315.
41. **Rhee, S.-Y., M. J. Gonzales, R. Kantor, B. J. Betts, J. Ravela, and R. W. Shafer.** 2003. HIV reverse transcriptase and sequence database. Nucleic Acids Res. **31:**298–303.
42. **Ridky, T., and J. Leis.** 1995. Development of drug resistance to HIV-1 protease inhibitors. J. Biol. Chem. **270:**29621–29623.
43. **Robinson, B. S., K. A. Riccardi, Y.-F. Gong, Q. Guo, D. A. Stock, W. S. Blair, B. J. Terry, C. A. Deminie, F. Djang, R. J. Colonno, and P.-F. Lin.** 2000. BMS-233632, a highly potent human immunodeficiency virus protease inhibitor that can be used in combination with other available antiretroviral agents. Antimicrob. Agents Chemother. **44:**2093–2099.
44. **Rosé, J. R., R. Salto, and C. S. Craik.** 1993. Regulation of autoproteolysis of the HIV-1 and HIV-2 protease with engineered amino acid substitutions. J. Biol. Chem. **268:**11939–11945.
45. **Sack, J. S., and F. A. Quiocho.** 1997. CHAIN-a crystallographic modeling program. Methods Enzymol. **277:**158–173.
46. Reference deleted.
47. **Sanne, I., P. Piliero, K. Squires, A. Thiry, and S. Schnittman.** 2003. Results of a phase 2 clinical trial at 48 weeks (A1424-007): a dose-ranging, safety, and efficacy comparative trial of atazanavir at three doses in combination with didanosine and stavudine in antiretroviral-naïve subjects. J. Acquir. Immune. Defic. Syndr. **32:**18–29.
48. **Satow, Y., G. H. Cohen, E. A. Padlan, and D. R. Davies.** 1986. Phosphocholine binding immunoglobulin Fab McPC603: an X-ray diffraction study at 2.7 Å. J. Mol. Biol. **190:**593–604.
49. **Schechter, I., and A. Berger.** 1967. On the size of the active site in protease. Biochem. Biophys. Res. Commun. **27:**157–162.
50. **Schinazi, R. F., B. A. Larder, and J. W. Mellors.** 1996. Mutations in retroviral genes associated with drug resistance. Int. Antiviral Newsl. **4:**95–107.
51. **Schnell, T., B. Schmidt, G. Moschik, C. Thein, C. Paatz, K. Korn, and H. Walter.** 2003. Distinct cross-resistance profiles of the new protease inhibitors amprenavir, lopinavir, and atazanavir in a panel of clinical samples. AIDS **17:**1324–1333.
52. **Shenderovish, M. D., R. M. Kagan, P. N. R. Heseltine, and K. Ramnarayan.** 2003. Structure-based phenotyping predicts HIV-1 protease inhibitor resistance. Protein Sci. **12:**1706–1718.
53. **Sheriff, S., and W. A. Hendrickson.** 1987. Description of overall anisotropy in diffraction from macromolecular crystals. Acta Crystallogr. A **43:**118–121.
54. **Starcich, B. R., B. H. Hahn, G. M. Shaw, P. D. McNeely, S. Modrow, H. Wolf, E. S. Parks, W. P. Parks, S. F. Josephs, R. C. Gallo, and F. Wong-Staal.** 1986. Identification and characterization of conserved and variable regions in the envelope gene of HTLV-III/LAV, the retrovirus of AIDS. Cell **45:**637–648.
55. **Todd, M. J., I. Luque, A. Velázquez-Campoy, and E. Freire.** 2000. The thermodynamic basis of resistance to HIV-1 protease inhibition: calorimetric analysis of the V82F/I84V active site resistant mutant. Biochemistry **39:**11876–11883.
56. **Vacca, J. P., and J. H. Contra.** 1997. Clinically effective HIV-1 protease inhibitors. Drug Discov. Today **2:**261–272.
57. **Vondrasek, J., C. P. van Buskirk, and A. Wlodawer.** 1997. Database of three-dimensional structures of HIV proteinases. Nat. Struct. Biol. **4:**8.
58. **Vondrasek, J., and A. Wlodawer.** 2002. HIVdb: a database of the structure of human immunodeficiency virus protease. Proteins **49:**429–431.
59. **Wallace, A. C., R. A. Laskowski, and J. M. Thornton.** 1995. LIGPLOT: a program to generate schematic diagrams of protein-ligand interactions. Protein Eng. **8:**127–134.
60. **Wang, Y.-X., D. I. Freedberg, T. Yamazaki, P. T. Wingfield, S. J. Stahl, J. D. Kaufman, Y. Kiso, and D. A. Torchia.** 1996. Solution NMR evidence that the HIV-1 protease catalytic aspartyl groups have different ionization states in the complex formed with the asymmetric drug KNI-272. Biochemistry **35:**9945–9950.
61. **Wang, Y.-X., D. I. Freedberg, S. Grzesiek, D. A. Torchia, P. T. Wingfield, J. D. Kaufman, S. J. Stahl, C.-H. Chang, and C. N. Hodge.** 1996. Mapping hydration water molecules in the HIV-1 protease/DMP323 complex in solution by NMR spectroscopy. Biochemistry **35:**12694–12704.
62. **Weinheimer, S., L. Discotto, J. Friborg, H. Yang, and R. Colonno.** 2005. Atazanavir signature I50L resistance substitution accounts for unique phenotype of increased susceptibility to other PIs in a variety of HIV-1 genetic backbones. Antimicrob. Agents Chemother. **49:**3816–3824.
63. **Wlodawer, A., and J. Vondrasek.** 1998. Inhibitors of HIV-1 protease: a major success of structure-assisted drug design. Annu. Rev. Biophys. Biomol. Struct. **27:**249–284.
64. **Wlodawer, A.** 2002. Rational approach to AIDS drug design through structural biology. Annu. Rev. Med. **53:**595–614.
65. **Yamazaki, T., L. K. Nicholson, D. A. Torchia, S. J. Stahl, J. D. Kaufman, P. T. Wingfield, P. J. Domaille, and S. Campbell-Burk.** 1994. Secondary structure and signal assignments of human-immunodeficiency-virus-1 protease complexed to a novel, structure-based inhibitor. Eur. J. Biochem. **219:**707–712.
66. **Yamazaki, T., A. P. Hinck, Y.-X. Wang, L. K. Nicholson, D. A. Torchia, P. Wingfield, S. J. Stahl, J. D. Kaufman, C.-H. Chang, P. J. Domaille, and P. Y. S. Lam.** 1996. Three-dimensional solution structure of the HIV-1 protease complexed with DMP323, a novel cyclic urea-type inhibitor, determined by nuclear magnetic resonance spectroscopy. Protein Sci. **5:**495–506.
67. **Yanchunas, J., D. R. Langley, L. Tao, R. E. Rose, J. Friborg, R. J. Colonno, and M. L. Doyle.** 2005. Molecular basis for increased susceptibility of atazanavir-resistant substitution I50L to other protease inhibitors. Antimicrob. Agents Chemother. **49:**3825–3832.